

Principles of the magnetic resonance imaging movie method for articulatory movement: a review

Midori Yoshida, Eiichi Honda, Erika Ozawa, Maristela Sayuri Inoue-Arai, Hiroko Ohmori, Keiji Moriyama,
Takashi Ono, Tohru Kurabayashi, Hozumi Yoshihara, Kulthida Nunthayanon Parakonthun

M Yoshida, E Honda, H Yoshihara

Department of Oral and Maxillofacial Radiology, University of Tokushima, Graduate School, 3-18-15
Kuramoto, Tokushima 770-8504, Japan

E Ozawa, H Ohmori, T Ono

Department of Orthodontic Science, Tokyo Medical and Dental University, Graduate School, Japan

MS Inoue-Arai, K Moriyama

Department of Maxillofacial Orthognathics, Tokyo Medical and Dental University, Graduate School, Japan

T Kurabayashi

Department of Oral and Maxillofacial Radiology, Tokyo Medical and Dental University, Graduate School, Japan

KN Parakonthun

Orthodontic Division, Department of Pedodontics & Preventive Dentistry, Faculty of Dentistry,
Srinakharinwirot University, Thailand

Corresponding author

Midori Yoshida

Department of Oral and Maxillofacial Radiology, University of Tokushima, Graduate School, 3-18-15
Kuramoto, Tokushima 770-8504, Japan

E-mail address: midori2@tokushima-u.ac.jp

Tel: +81-88-633-7361; Fax: +81-88-633-5335

Conflict of interest

Midori Yoshida, Eiichi Honda, Erika Ozawa, Maristela Sayuri Inoue-Arai, Hiroko Ohmori, Keiji Moriyama, Takashi Ono, Tohru Kurabayashi, Hozumi Yoshihara, and Kulthida Nunthayanon Parakonthun declare that they have no conflict of interest.

Human rights statement and informed consent

All procedures followed were in accordance with the ethical standards of the responsible committee on human experimentation (institutional and national) and with the Helsinki Declaration of 1964 and later versions.

Informed consent was obtained from all patients for being included in the study. The research was approved by the Institutional Ethical Review Board of the Tokyo Medical and Dental University (number 1282).

Acknowledgment

This study was supported by JSPS KAKENHI Grant Number JP16K1150800.

Abstract

Magnetic resonance imaging (MRI) has become a critical tool for dental examination. MRI has many advantages over radiographic examination methods, including the lack of a requirement for patient exposure and the ability to capture high-contrast images of various tissue and organ types. However, MRI also has several limitations, including long examination times and the existence of metallic or motion artifacts. A cardiac imaging method using cine sequences was developed in the 1990s. This technique allows for analysis of heart movement and functional blood flow. Moreover, this method has been applied in dentistry. Recent research involving 3T MRI has led to the achievement of a temporal resolution of <10 ms, surpassing the frame rate of typical video recording. The current review introduces the history and principles of the cine sequence method and its application to the oral and maxillofacial regions.

Keywords: Segmented k-space cine sequence, artifact, pronunciation, teeth

Introduction

The development of magnetic resonance imaging (MRI) was based on nuclear magnetic resonance (NMR) research performed by Bloch et al. [1] and Purcell et al. [2] in the 1940s. Many promising results of NMR research were subsequently reported, and Nobel prizes were awarded to researchers in the field, including the two above-mentioned research groups [3]. MRI is an imaging technology that utilizes NMR and was initially proposed and developed by Mansfield and Maudsley [4] and Lauterbur [5]. MRI has become an essential imaging modality for diagnosis in medicine. Most technological development of MRI has focused on enhancing the static magnetic field strength to improve the signal-to-noise ratio and spatial resolution. The spatial resolution of current MRI scanners is superior to that of computed tomography (CT) scanners, and scanners exceeding 10T have recently been developed. Research with 11.7T MRI was reported in 2000 [6]. In 2006, 17.6T MRI scanning was reported [7]. Although these studies have typically been performed with animals, 39-potassium 9.4T MRI of the human brain was performed in 2014 [8]. However, the maximum static magnetic field strength of clinical scanners is currently 7T. MRI scanners with greater magnetic field strength can display images of very small structures, while conventional scanners cannot gain a signal from hard tissue because the T2 value of hard tissue is very low. Therefore, hard tissues such as teeth cannot be visualized using conventional MRI.

In dentistry, CT scanning has become widespread as an appropriate modality because the main targets of diagnosis are hard tissues, including teeth and bone in the oral and maxillofacial regions. MRI of the temporomandibular joint disk was first reported in the mid-1980s, and MRI has since become the most important modality in dentistry for diagnosis of temporomandibular disorders [9, 10]. The disk position and joint morphology can be diagnosed by MRI. New tooth-imaging research methods have recently been reported using a high-strength magnetic field scanner, enabling clear MR images that can discriminate enamel, dentin, and pulp [11]. Ultra-high magnetic fields can greatly shorten the echo time (TE). By shortening the TE to less than the T2 value of the tissue, even hard tissues can be imaged. This new approach is called the ultra-short TE sequence (UTE) or zero TE sequence (ZTE). Whereas teeth cannot be imaged with conventional MRI, imaging is enabled by UTE or ZTE with ultra-high magnetic field strength, such as that provided by 11.7T scanners.

In addition to tooth imaging, several other types of useful imaging-related techniques have been applied in dentistry. Functional MRI of tongue movement, which can measure brain activity and create brain maps of signals, has been described since the early 2000s [12, 13]. This method is based on the blood oxygen level-dependent (BOLD) effect discovered by Ogawa et al. [14]. Research has revealed significant relationships

among brain activity, tongue movement, and chewing.

MRI has become widely used in dentistry and has the advantage of requiring no patient exposure, unlike CT. However, some disadvantages of MRI also exist. One limitation is the appearance of large signal-void areas caused by the presence of internal metals (i.e., metallic artifact). MRI diagnosis may be impossible depending on the type of metal involved. Many studies have been performed to examine biomaterials, and MR-compatible alloys in which niobium or zirconium is added to gold and platinum with very low magnetic susceptibility have been developed [15, 16]. These alloys show no metallic artifacts and are expected to be used clinically in future.

Another important problem is that imaging times are often very long for MRI. More than 100 slice images can be obtained within 1 s by modern CT scanners; this imaging rate cannot be achieved with MRI. The imaging time of MRI greatly depends on the sequence used. Echo planar imaging (EPI) is considered the fastest sequence, but this sequence is not used in the diagnosis of anatomical structures because its spatial and tissue resolution are low. The fast spin echo sequence (FSE) and gradient echo sequence (GRE) are routinely used, with imaging times exceeding 1 min. This problem is very difficult to resolve.

In medical research, MRI has been widely used for heart examination. Because the heart produces approximately one heartbeat per second, there is no general sequence that can accurately image cardiac movement. Assessing cardiac movement requires continuous images obtained at the same cross section with a temporal resolution of a few tens of milliseconds. The cine MRI technique makes it possible to assess the flow and function in the heart and vessels. Cine MRI with a modified electrocardiography-gated two-dimensional discrete Fourier transform method was first reported in 1985 and had an imaging time of 8 minutes [17]. The temporal resolution was increased to 20 ms by the spin echo sequence (SE) [18]. In 1987, cine MRI of the heart using GRE was reported [19]. A new technique involving the filling of k-space was then developed to further shorten the imaging time in the 1990s. This method is called segmented k-space cine MRI [20, 21]. In early studies of cine MRI, a 1.5T scanner was used. Since the 2000s, however, 3T scanners have been used [22].

Currently, temporal resolution can be increased to 10 ms by increasing the static magnetic field strength of scanners and the repeat count of movements. Thus, the imaging time has been substantially shortened. Cine MRI techniques are also very useful in dentistry. Applying the technique to the oral and maxillofacial regions has enabled dynamic analysis of pronunciation and utterance. Fluoroscopic images are usually used for dynamic analysis. However, these methods involve some level of patient exposure, and only two-dimensional projection images can be obtained. The development of methods with which to analyze these

images using cine MRI could potentially overcome these limitations.

Imaging time in MRI

Imaging time of MRI mainly depends on the repetition time (TR), number of phase-encoding steps (N[phase]), and number of excitations (N[excitation]). Because N(phase) determines only one side of the matrix size, the relationship between time and size is not always proportional. When collecting NMR signals, encoding is required to determine spatial position. The encoding is performed for the x- and y-axes, and these are called phase and frequency encoding. The NMR signal, including information of encoding, becomes the MRI signal. The time required for phase encoding is substantially longer than that required for frequency encoding, and the imaging time is mainly determined by N(phase). The increase in the number of frequency-encoding steps (N[frequency]) has little effect on the time required. Thus, the imaging time is proportional to N(phase) and is almost independent of N(frequency). The relationship is expressed by the following equation.

$$\text{Imaging time} = \text{TR} \times \text{N(phase)} \times \text{N(excitation)}$$

Sequences are roughly divided into two types: SE and GRE (Fig. 1) [23]. After the time interval between the two radiofrequency (RF) pulses, spin echo can be observed. The general time interval is in the order of hundreds of milliseconds, and the imaging time is approximately 1 minute when N(phase) is 128 (2^7 is basic). In GRE, magnetic field inversion is used instead of the 180° RF pulse (Fig. 2). Gradient echo is immediately generated even if the time interval between α° RF pulse and magnetic field inversion is very short, in the order of several milliseconds. The same number of α° RF pulses as in N(phase) is required in GRE. Therefore, even if the minimum interval is used, the imaging time is hundreds of milliseconds. EPI can be used to further shorten the imaging time. The imaging time can be shortened by magnetic field inversion after one α° RF pulse. EPI is the fastest imaging sequence, enabling an imaging time of approximately 10 ms per slice. However, imaging time and image quality typically have a tradeoff relationship: generally, the shorter the imaging time, the lower the image quality. Because EPI images have some specific artifacts, these images are routinely used not for anatomical diagnosis but instead for functional diagnosis. Substantial image distortion arises when examining structures of very different magnetic susceptibility. Because magnetic susceptibility is very different between soft tissue and air (e.g., in the sinus, nasal cavity, and oral cavity in the oral and maxillofacial regions), diagnosis with EPI images is impossible. Thus, FSE and GRE are generally used.

Cine MRI

The cine mode in medicine is a method of continuously displaying static images obtained at constant short time intervals. The shorter the time interval, the smoother the subjects' movement becomes. When a time interval is long, image blurring arises. The name "cine" is derived from "cinema," and digital video similarly involves the display of a series of static images. Standard video typically involves 30 frames (images) per second, with a time interval of 33 ms (1/30). The time interval gives the temporal resolution. Continuous static images obtained in a very short time are required to enable cine mode in MRI.

It is not possible to obtain continuous images with a temporal resolution of 30 ms using GRE because of the limitations in shortening the TR. In the conventional k-space filling method, the same number of TRs as $N(\text{phase})$ are used in one movement, such as a heartbeat (Fig. 3). The image is blurred because an obtained image includes movement during the time ($\text{TR} \times N(\text{phase})$) required to fill k-space. One method for increasing the temporal resolution is to fill each line of k-space with repetitive movement (Fig. 4). By repeating the same number of movements as $N(\text{phase})$, all lines of k-space have the same temporal resolution as the TR. Regular repetitive movement is required to apply this method. The time interval of movements is generally substantially longer than the TR, and many images at different times can then be obtained by adding more RF pulses in the vacant time. Thus, continuous images at different times can be obtained by preparing many k-spaces and filling each k-space line by line with one movement, meaning that images have a temporal resolution of the TR (Fig. 5). Cine MRI is completed by consecutively displaying the images. The technique was initially developed for diagnosis of the heart and vessels because the heart regularly beats, requiring short temporal resolution. It is also very important to match the starting point of each movement. The timing to start scanning is determined by two methods: one is to measure the R-wave of the electrocardiogram and synchronize the heartbeat with the starting point of TR, and the other method is to use an external trigger signal. In the latter method, scanning can start from any point regardless of heartbeat. One slice imaging of the heart takes approximately 2 minutes when the $N(\text{phase})$ is 128 and the heart rate is 60 beats/min.

A new technique was subsequently developed to further shorten the imaging time. In this technique, multiple lines of k-space are filled at one TR (Fig. 6). When the number of multiple lines is $N(\text{segment})$, the imaging time or repeat count of movement is reduced to $1/N(\text{segment})$. $N(\text{segment})$ is called the "number of segments" by Siemens (Munich, Germany) and the "views per segment" by GE Healthcare (Chicago, IL, USA). This technique is known as segmented k-space cine MRI. However, the temporal resolution becomes longer with the increase in $N(\text{segment})$ because temporal resolution is proportional to $N(\text{segment})$. GRE using steady-state free precession (SSFP) is routinely used in segmented k-space cine MRI. GRE can shorten the TR

to several milliseconds, and a temporal resolution of 30 ms can be achieved [24]. Moreover, it is possible to further shorten the imaging time without deterioration of image quality using parallel imaging techniques [25].

Application of cine MRI to oral and maxillofacial regions

In the oral and maxillofacial regions, analysis of pronunciation function is an important issue. Articulatory organs including the tongue, lips, and soft palate are soft tissues, and dynamic function of the anatomical outline has traditionally been evaluated using video-fluorography. In cardiac diagnosis, segmented k-space cine MRI has proven useful for diagnosis of articulatory movement because it requires no patient exposure. This method is also known as the MRI movie approach in the oral and maxillofacial regions, and studies of this technique have been reported since the late 1990s [26]. Many other studies of articulatory movement during pronunciation by 1.5T MRI have since been reported [27-32], and several recent studies have used 3T MRI [33-36].

The movements of most organs other than the heart are voluntary, and it is difficult to control the regularity of movement. Irregular movement creates distorted images; thus, an important issue in cine MRI is the method of repeating a movement. Rhythmical audio signals have been utilized for rhythmical repetition of speech and pronunciation [26, 27]. Using this method, the subject performs a movement in time with the rhythmic signal. Rhythmical movement can be easily achieved with a short training period: a subject listens to the audio signal in the MR gantry with MR-compatible headphones and repeats a specific pronunciation a predetermined number of times according to the signal. The starting point of scanning is determined by an external trigger signal. The audio and trigger signals are synchronized. This technique requires the capability to start scanning using an external trigger signal and a specific apparatus to generate both a synchronized trigger and rhythmical signals (Figs. 7, 8).

A segmented k-space cine sequence greatly reduces the repeat count of movements. Temporal resolution (R_t) and repeat count (Cr) depend on $N(\text{segment})$. The product of R_t and Cr is a constant. R_t in the sequence refers to the TR. R_t is determined by the extent to which the researcher wishes to analyze a movement. In the analysis of tongue movement during pronunciation, a difference has been reported between temporal resolution of 30 ms and <30 ms [34]. The relationship among R_t , Cr , and $N(\text{segment})$ depends on the performance of scanners. In our studies involving 3T MRI, we have expressed this using the following equations when $N(\text{phase})$ is 256 using the GRAPPA algorithm [33-36]:

$$R_t = N(\text{segment}) \times 4.5$$

$$N(\text{segment}) \times Cr = 120$$

To set R_t at 45 ms, $N(\text{segment})$ is 10 and Cr is calculated as 12. In our experience, subjects find it relatively easy to regularly repeat pronunciation 12 times, and R_t of 10 ms can be achieved.

Figures 9 to 11 show the difference in image quality during pronunciation caused by the difference in R_t . Image quality with R_t of 135 ms is superior to that of 45 ms when the tongue is at rest. In contrast, image quality with R_t of 135 ms decreases during movement. A shorter TR reduces the signal-to-noise ratio, and an image for 135 ms has 1.7 times this ratio compared with an image for 45 ms. Therefore, image quality improves due to noise reduction. However, when the tongue moves faster than 135 ms, the first and last images for 45 ms have different tongue positions. As a result, adding images at different times produces distortion around the tongue. R_t should be determined according to the movement speed. In recent research on pronunciation, R_t of <30 ms is used in 3T MRI [33-36].

A method of compressed sensing was recently introduced to reduce the MRI acquisition time [37]. Compressed sensing accelerates data acquisition by collecting fewer data. Parallel imaging is routinely used to reduce the acquisition time, but an acceleration factor of ≥ 3 causes image degradation because of a decrease in the signal-to-noise ratio. In compressed sensing, the degradation of image quality is very small even with an acceleration factor of ≥ 10 . Moreover, compressed sensing can be used simultaneously with parallel imaging, and it is used for cardiac and body imaging in the clinical setting. Compressed sensing cardiac cine is now available, and a cardiac cine scan can be completed within 25 seconds according to Siemens [38]. The authors believe that compressed sensing can also be applied to the MRI movie technique in the oral and maxillofacial region.

Visualization of teeth and recording of sound data

Conventional MRI can depict soft tissues, but hard tissues such as teeth cannot be visualized because the T2 value of teeth is very short. A new MRI method using UTE and ZTE makes it possible to visualize teeth but requires a scanner of 7T or more [11]. However, it is not currently possible to adapt this method to patients in clinical situations.

A practical method for visualizing teeth has been reported [27]. Tooth contours can be depicted using agar containing contrast agent in an individual plastic tray. The food additive ammonium ferric citrate (15 mg) is used as the contrast agent, and the food additive sodium hydrogen carbonate is added as a pH-adjusting agent. An image of the teeth can be obtained by superimposing the tooth image on a conventional image in which the tooth is not visualized (Fig. 12). Three markers containing 8 mg/mL of an aqueous solution of ammonium ferric

citrate are used as superimposition markers.

Analyzing sound data during pronunciation is also an important issue. An MRI-compatible microphone is necessary for the MRI movie method and has unique requirements. MRI produces a loud noise, and the frequency is characteristic. The system can reduce the noise using a digital sound processor. The signal of the subjects' pronunciation is sent through an optical fiber and converted to an electrical signal outside the scanner room. Sound wave data can be obtained by overlapping the electric signal and the trigger signal to which the subject pronounces in response (Fig. 13).

Difference of sequence in MRI movie method

SE and GRE can be used even in the MRI movie method if software supports a cine sequence. GRE has generally been used because the shorter TR can improve the temporal resolution. GRE has some variations and is mainly classified into two types: coherent and incoherent. Coherent refers to the effect of residual transverse magnetization after applying an RF pulse, and an incoherent sequence spoils the transverse magnetization.

Fast low-angle shot (FLASH) is an incoherent GRE in Siemens scanners. This method is also called spoiled gradient recalled acquisition in the steady state (SPGR or spoiled GRASS) in GE scanners (Fig. 14). The residual transverse magnetization is spoiled by continuous shifting of RF pulses or magnetic field gradients.

Fast imaging with steady-state precession (FISP) is a coherent GRE method that involves a rewinder in the phase-encoding direction (Fig. 15). In GRE, transverse magnetization remains after applying the RF pulse, and residual transverse magnetization is conserved after applying many RF pulses with a short TR. Both the longitudinal and transverse magnetization are constant. This method is called SSFP. Coherent GRE actively utilizes transverse magnetization in SSFP. The rewinder refocuses the residual transverse magnetization and maintains coherence. It is called GRASS in GE scanners.

True FISP is also a coherent GRE method and has a fully balanced gradient waveform by each rewinder in three directions of slice, readout, and phase encodings. Compared with FISP, two more rewinders are added and used for two stages before applying the RF pulse and after reading signals (Fig. 16). Therefore, signals of free induction decay, spin echo, and stimulated spin echo are overlapped in the same phase, and the signal intensity increases. True FISP uses the three signals, while FISP targets only the free induction decay signal. This technique is called fast imaging employing steady-state acquisition (FIESTA) in GE scanners.

FLASH of these three GRE methods is routinely used for analysis of pronunciation in the MRI movie approach. The outline of the lips, tongue, soft palate, and pharyngeal tissue are clearly observed in T1-weighted

images (Fig. 17a). True FISP is generally used in cardiac cine MRI because the TR can be further shortened and the blood flow signals can be obtained. However, true FISP is not suitable for MRI movie examination of the oral and maxillofacial regions. The water signal intensity, including that of cerebrospinal fluid, is too high, and the signal intensity of soft tissues is relatively low; thus, it is difficult to discriminate the outline of soft tissues related to pronunciation (Fig. 17b). Moreover, a specific band artifact causing a black line appears at random in true FISP. The outline of tissues may be changed by the line. The position of the line can be shifted by changes in the receiver bandwidth frequency. However, removal of all lines from the area of interest in the oral regions was impossible in our previous study. This may be a particular phenomenon in the oral and maxillofacial regions because of the very different magnetic susceptibility of air and tissue.

In FISP images, the signal intensity of the cerebrospinal fluid is relatively low, but that of the tongue and soft palate are also low compared with FLASH images (Fig. 17c). FLASH images are currently considered to exhibit the best performance in the MRI movie method.

Metallic artifacts in the MRI movie method

Metallic artifacts do not typically need to be considered in cardiac cine MRI. However, many metallic restorations such as inlays, crowns, screw posts, and dental implants are used in dental treatment. Metallic materials may cause image distortion or signal void. The extent of the artifact depends on the magnetic susceptibility and weight of the metals. Gold reportedly has little influence, whereas the titanium used in dental implants has some influence [39]. Recent research has suggested that soft tissue measurements in MRI movie examination can significantly fluctuate depending on the type of orthodontic metallic appliance [15]. Metallic orthodontic appliances produce large artifacts in the MRI movie method. Typical fixed retainers and metal brackets cause a loss of signal intensity of the lips, tongue apex, and palate [36].

Conclusion

The MRI movie method using a segmented k-space cine sequence is a very useful technology in the dynamic analysis of pronunciation, achieving a temporal resolution of <10 ms. Moreover, the burden on the subjects is relatively light, and the absence of a need for patient exposure is an important advantage over X-ray fluoroscopy. Although the present paper presented only sagittal MRI movie images, the method is easy to apply in any direction. The development of an external trigger function and a built-in segmented k-spaced cine sequence would enable the MRI movie method to be used for a range of useful applications. The authors hope that in

order to reduce medical exposure, this method will be widely applied to dynamic analysis instead of methods using X-ray.

References

1. Bloch F, Hansen WW, Packard M. Nuclear Induction. *Phys Rev.* 1946;69:127.
2. Purcell EM, Torrey HC, Pound RV. Resonance absorption by nuclear moments in a solid. *Phys Rev.* 1946;69:37–8.
3. Yoshida M, Honda E. Trends in magnetic resonance imaging research in dentistry. *Dent Health Curr Res.* 2015;1:2. doi:10.4172/2470-0886.1000e104.
4. Mansfield P, Maudsley AA. Medical imaging by NMR. *Br J Radiol.* 1977;50:188–94.
5. Lauterbur PC. Progress in n.m.r. zeugmatography imaging. *Philos Trans R Soc Lond B Biol Sci.* 1980;289:483–7.
6. Dubowitz DJ, Tyszkaj JM, Sewry CA, Moats RA, Scadeng M, Dubowitz V. High resolution magnetic resonance imaging of the brain in the dy/dy mouse with merosin-deficient congenital muscular dystrophy. *Neuromuscul Disord.* 2000;10:292–8.
7. Weber T, Vroemen M, Behr V, Neuberger T, Jakob P, Haase A, et al. In vivo high-resolution MR imaging of neuropathologic changes in the injured rat spinal cord. *Am J Neuroradiol.* 2006;27:598–604.
8. Atkinson DJ, Edelman RR. Cineangiography of the heart in a single breath hold with a segmented turboFLASH sequence. *Radiology.* 1991;178:357–60.
9. Roberts D, Schenck J, Joseph P, Foster T, Hart H, Pettigrew J, et al. Temporomandibular joint: magnetic resonance imaging. *Radiology.* 1985;154:829–30.
10. Katzberg RW. Temporomandibular joint imaging. *Radiology.* 1989;170:297–307.
11. Weiger M, Pruessmann KP, Bracher AK, Köhler S, Lehmann V, Wolfram U, et al. High-resolution ZTE imaging of human teeth. *NMR Biomed.* 2012;25:1144–51.
12. Shinagawa H, Ono T, Ishiwata Y, Honda E, Sasaki T, Taira M, et al. Hemispheric dominance of tongue control depends on the chewing-side preference. *J Dent Res.* 2003;82:278–83.
13. Shinagawa H, Ono T, Honda E, Sasaki T, Taira M, Iriki A, et al. Chewing-side preference is involved in differential cortical activation patterns during tongue movements after bilateral gum-chewing: a functional magnetic resonance imaging study. *J Dent Res.* 2004;83:762–6.
14. Ogawa S, Lee TM, Kay AR, Tank DW. Brain magnetic resonance imaging with contrast dependent on blood oxygenation. *Proc Natl Acad Sci U S A.* 1990;87:9868–72.
15. Uyama E, Inui S, Hamada K, Honda E, Asaoka K. Magnetic susceptibility and hardness of Au-xPt-yNb

- alloys for biomedical applications. *Acta Biomater.* 2013;9:8449–53.
16. Li HF, Zhou FY, Li L, Zheng YF. Design and development of novel MRI compatible zirconium-ruthenium alloys with ultralow magnetic susceptibility. *Sci Rep.* 2016;6:24414. doi:10.1038/srep24414.
 17. Waterton JC, Jenkins JP, Zhu XP, Love HG, Isherwood I, Rowlands DJ. Magnetic resonance (MR) cine imaging of the human heart. *Br J Radiol.* 1985;58:711–6.
 18. Sechtem U, Pflugfelder P, Higgins CB. Quantification of cardiac function by conventional and cine magnetic resonance imaging. *Cardiovasc Intervent Radiol.* 1987;10:365–73.
 19. Sechtem U, Pflugfelder PW, White RD, Gould RG, Holt W, Lipton MJ, et al. Cine MR imaging: potential for the evaluation of cardiovascular function. *AJR Am J Roentgenol.* 1987;148:239–46.
 20. Bluemke DA, Boxerman JL, Atalar E, McVeigh ER. Segmented K-space cine breath-hold cardiovascular MR imaging: Part 1. Principles and technique. *AJR Am J Roentgenol.* 1997;169:395–400.
 21. Ridgway JP. Cardiovascular magnetic resonance physics for clinicians: part 1. *J Cardiovasc Magn Reson.* 2010;12:71.
 22. Gilson WD, Kraitchman DL. Cardiac magnetic resonance imaging in small rodents using clinical 1.5 T and 3.0 T scanners. *Methods.* 2007;43:35–45.
 23. Siemens Healthcare. Bandwidth in MRI? http://dev.clinical-mri.com.s166757.gridserver.com/wp-content/uploads/software_hardware_updates/Flash_52_HIDI_Bandwidth_13_03_19.pdf (accessed May 2018)
 24. Kunz RP, Oellig F, Krummenauer F, Oberholzer K, Romaneehsen B, Vomweg TW, et al. Assessment of left ventricular function by breath-hold cine MR imaging: comparison of different steady-state free precession sequences. *J Magn Reson Imaging.* 2005;21:140–8.
 25. Wintersperger BJ, Nikolaou K, Dietrich O, Rieber J, Nittka M, Reiser MF, et al. Single breath-hold real-time cine MR imaging: improved temporal resolution using generalized autocalibrating partially parallel acquisition (GRAPPA) algorithm. *Eur Radiol.* 2003;13:1931–6.
 26. Masaki S, Tiede MK, Honda K, Shimada Y, Fujimoto I, Nakamura Y, et al. MRI-based speech production study using a synchronized sampling method. *J Acoust Soc Jpn.* 1999;20:375–9.
 27. Ng IW, Ono T, Inoue-Arai MS, Honda E, Kurabayashi T, Moriyama K. Differential articulatory movements during Japanese /s/ and /t/ as revealed by MR image sequences with tooth visualization.

- Arch Oral Biol. 2012;57:749–59.
28. Shinagawa H, Ono T, Honda E, Masaki S, Shimada Y, Fujimoto I, et al. Dynamic analysis of articulatory movement using magnetic resonance imaging movies: methods and implications in cleft lip and palate. *Cleft Palate Craniofac J.* 2005;42:225–30.
 29. Sato-Wakabayashi M, Inoue-Arai MS, Ono T, Honda E, Kurabayashi T, Moriyama K. Combined fMRI and MRI movie in the evaluation of articulation in subjects with and without cleft lip and palate. *Cleft Palate Craniofac J.* 2008;45:309–14.
 30. Inoue MS, Ono T, Honda E, Kurabayashi T. Characteristics of movement of the lips, tongue and velum during a bilabial plosive: a noninvasive study using a magnetic resonance imaging movie. *Angle Orthod.* 2007;77:612–8.
 31. Inoue MS, Ono T, Honda E, Kurabayashi T, Ohyama K. Application of magnetic resonance imaging movie to assess articulatory movement. *Orthod Craniofac Res.* 2006;9:157–62.
 32. Ng IW, Ono T, Inoue-Arai MS, Honda E, Kurabayashi T, Moriyama K. Application of MRI movie for observation of articulatory movement during a fricative /s/ and a plosive /t/. *Angle Orthod.* 2011;81:237–44.
 33. Nunthayanon K, Honda E, Ohmori H, Inoue-Arai MS, Shimazaki K, Kurabayashi T, et al. A pilot study on characterization of articulatory movements during fricative /s/ sound in an anterior open bite subject: a tooth-visualized 3-T MRI movie evaluation. *J World Feder Orthod.* 2015;4:71–7.
 34. Nunthayanon K, Honda E, Shimazaki K, Ohmori H, Inoue-Arai MS, Kurabayashi T, et al. Use of an advanced 3-T MRI movie to investigate articulation. *Oral Surg Oral Med Oral Pathol Oral Radiol.* 2015;119:684–94.
 35. Nunthayanon K, Honda E, Shimazaki K, Ohmori H, Inoue-Arai MS, Kurabayashi T, et al. Differences in velopharyngeal structure during speech among Asians revealed by 3-Tesla magnetic resonance imaging movie mode. *Biomed Res Int.* 2015;2015:126264.
 36. Ozawa E, Honda EI, Parakonthun KN, Ohmori H, Shimazaki K, Kurabayashi T, et al. Influence of orthodontic appliance-derived artifacts on 3-T MRI movies. *Prog Orthod.* 2018;19:7.
 37. Jaspán ON, Fleysher R, Lipton ML. Compressed sensing MRI: a review of the clinical literature. *Br J Radiol.* 2015;88:20150487.
 38. Siemens Healthineers. Compressed sensing cardiac cine.
<https://www.healthcare.siemens.com/magnetic-resonance-imaging/options-and-upgrades/clinical-applic>

ations/compressed-sensing-cardiac-cine#. (accessed 2018 August)

39. Shafiei F, Honda E, Takahashi H, Sasaki T. Artifacts from dental casting alloys in magnetic resonance imaging. *J Dent Res.* 2003;82:602–6.

Figure legends

Fig. 1 Sequence timing diagram of spin echo sequence by Siemens. Horizontal and vertical directions of each graph show the time and magnitude of the gradient. The matrix size is 256×256

Fig. 2 Sequence timing diagram of typical gradient echo sequence

Fig. 3 Conventional k-space filling method. One line of k-space is filled with one repetition time (TR). The number of phase-encoding steps is 128, and the same number of TRs is required to fill all lines of k-space. Only a single cardiac phase is obtained. The time resolution and imaging time are $128 \times TR$

Fig. 4 Principle of k-space filling by a cine sequence. One line of k-space is filled with one heartbeat and one repetition time (TR). Only a single cardiac phase is obtained. The time resolution is the TR, but the imaging time is $128 \times (R-R \text{ interval})$

Fig. 5 Principle of multiphase cardiac cine sequence. Eight k-spaces from A to H are prepared, and 8 cardiac phases (images) from A to H can be obtained by 128 heartbeats. One line of eight k-spaces from A to H is filled with one heartbeat and one repetition time (TR) because the TR is much shorter than the R-R interval. Eight cardiac phases are obtained. The temporal resolution of each cardiac phase is the TR, but the imaging time is $128 \times (R-R \text{ interval})$

Fig. 6 Principle of segmented k-space cine sequence. Eight k-spaces from A to H are prepared, and 8 cardiac phases from A to H can be obtained by only 16 heartbeats. Eight lines of eight k-spaces from A to H are filled with one repetition time (TR). The TR is eight times longer than the TR in Figure 5. Although the imaging time is shortened to $16 \times (\text{R-R interval})$, the temporal resolution is extended to eight times that in Figure 5. Thick lines representing cardiac phases from A to H show that the time resolution is long

Fig. 7 Signal transmission paths in magnetic resonance imaging (MRI) movie system. (1) A personal computer (PC) generates a trigger pulse and a tone burst signal. The pulse and signal are sent to an MRI scanner and a digital recorder. The MRI scanner starts according to the trigger pulse. (2) The subject listens to the sound of the tone burst signal with headphones and performs the pronunciation. (3) The pronunciation is sent to the digital recorder, with which it is recorded

Fig. 8 Diagram of k-space filling in magnetic resonance imaging movie method. The segmented k-space sequence is used. The starting point of scanning is determined by an external trigger signal. The subject repeats pronunciation of /apa/ according to the audio signal from headphones. Continuous images can be obtained

Fig. 9 Magnetic resonance movie images almost at rest. Image (a) has good image quality with less noise, but image (b) has slight roughness. (a) Repetition time of 135 ms. (b) Repetition time of 45 ms. (c) Magnification of

image a. (d) Magnification of image b

Fig. 10 Magnetic resonance movie images during movement. (a) Repetition time of 135 ms. The soft palate is blurred and the outline of the lower lip is unclear. (b) Repetition time of 45 ms. (c) Magnification of image a. (d) Magnification of image b

Fig. 11 Continuous magnetic resonance movie images. (a–d) Repetition time of 135 ms. (e–h) Repetition time of 45 ms. The elapsed time in images e, f, g, and h corresponds to that in images a, b, c, and d.

Fig. 12 Magnetic resonance movie image with tooth image. (a) T1-weighted image by turbo spin echo image using three markers (forehead, nose, and chin surface) and individual trays of both upper and lower jaws. The trays are filled with gel including ammonium ferric citrate, and a high-intensity signal can be observed. (b) Tooth images (yellow) are created by software. (c) Magnetic resonance movie image by fast low-angle shot. The teeth cannot be observed. (d) The tooth images are superimposed on image c.

Fig. 13 Sound signal and magnetic resonance movie images with teeth. The graph shows sound data during pronunciation of /apa/. The vertical and horizontal axes show the signal intensity of the sound data and time.

Fig. 14 Sequence timing diagram of fast low-angle shot. The radiofrequency (RF) pulse includes spoiler

(RF-spoiling). Spoiler gradients are also added to each direction of G_x , G_y , and G_z .

Fig. 15 Sequence timing diagram of fast imaging with steady-state precession. Rewinder is added to the phase-encoding direction (G_y)

Fig. 16 Sequence timing diagram of true fast imaging with steady-state precession (FISP). Two rewinders are also added to the direction of G_z and G_x compared with FISP. Gradients of both G_z and G_x become symmetrical by adding rewinders. This sequence is also called the balanced steady-state free precession sequence.

Fig. 17 Comparison of magnetic resonance movie images by different sequences. (a) Fast low-angle shot image. (b) True fast imaging with steady-state precession (FISP) image. (c) FISP image

Figure 1

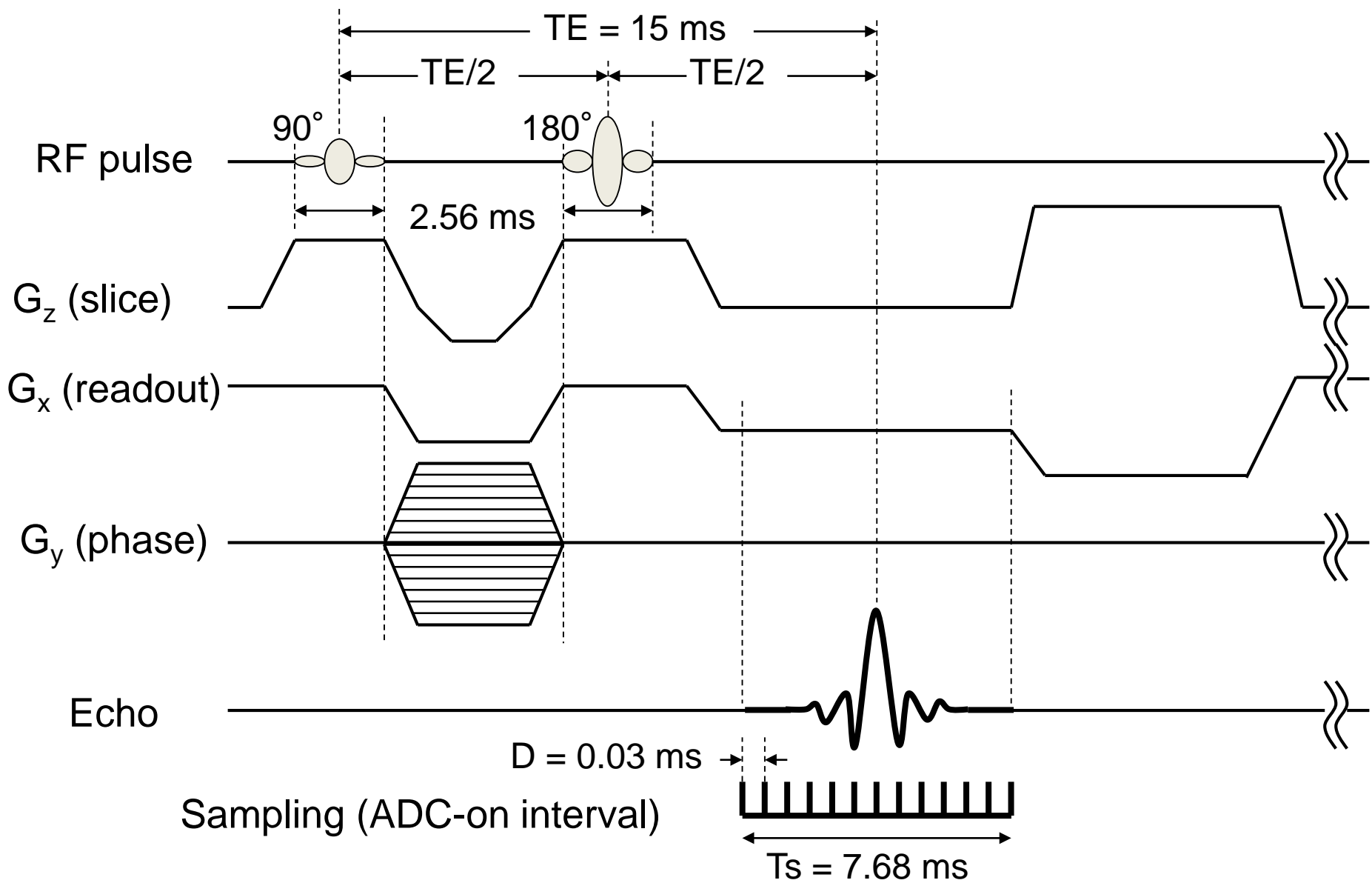


Figure 2

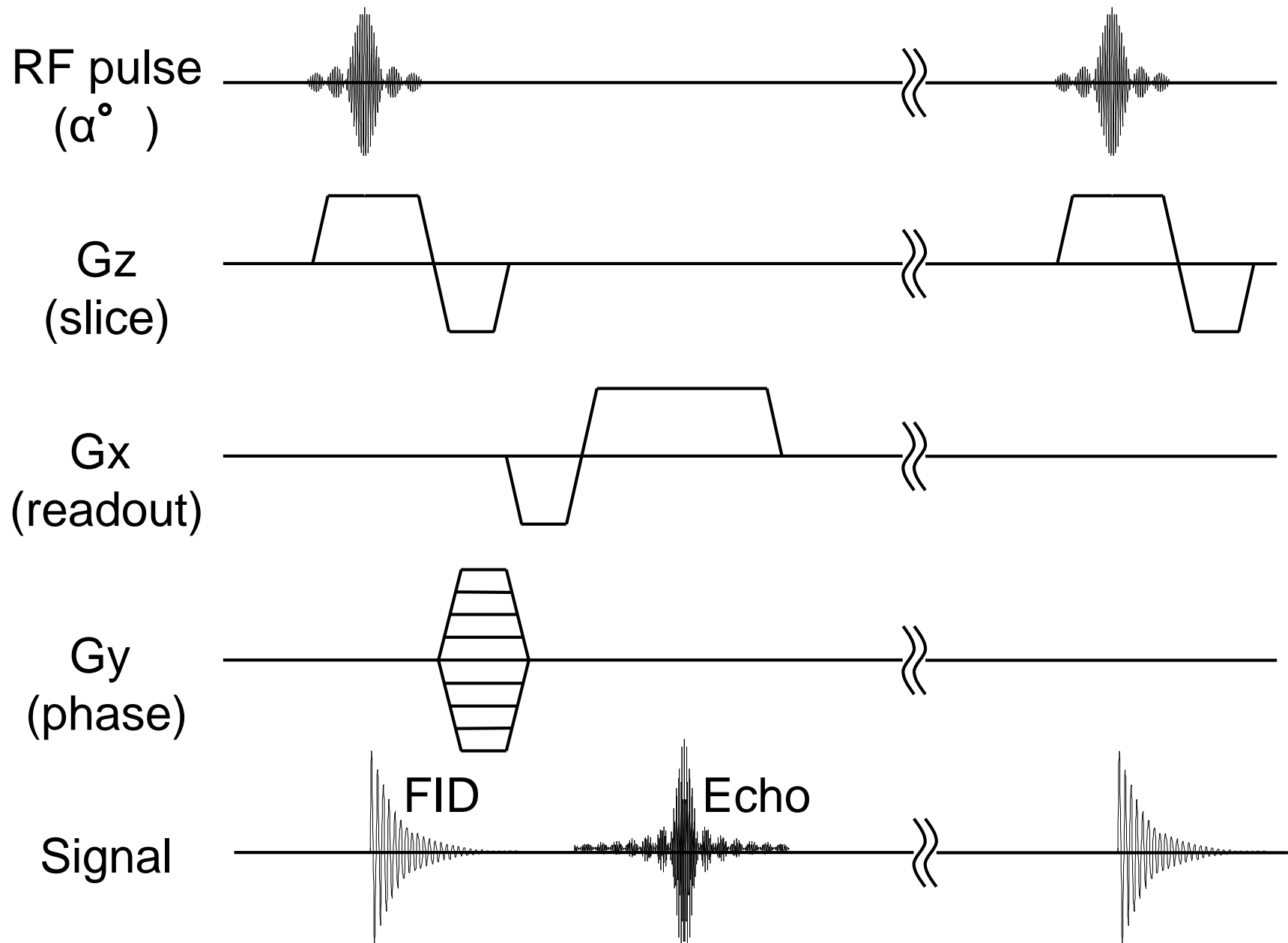


Figure 3

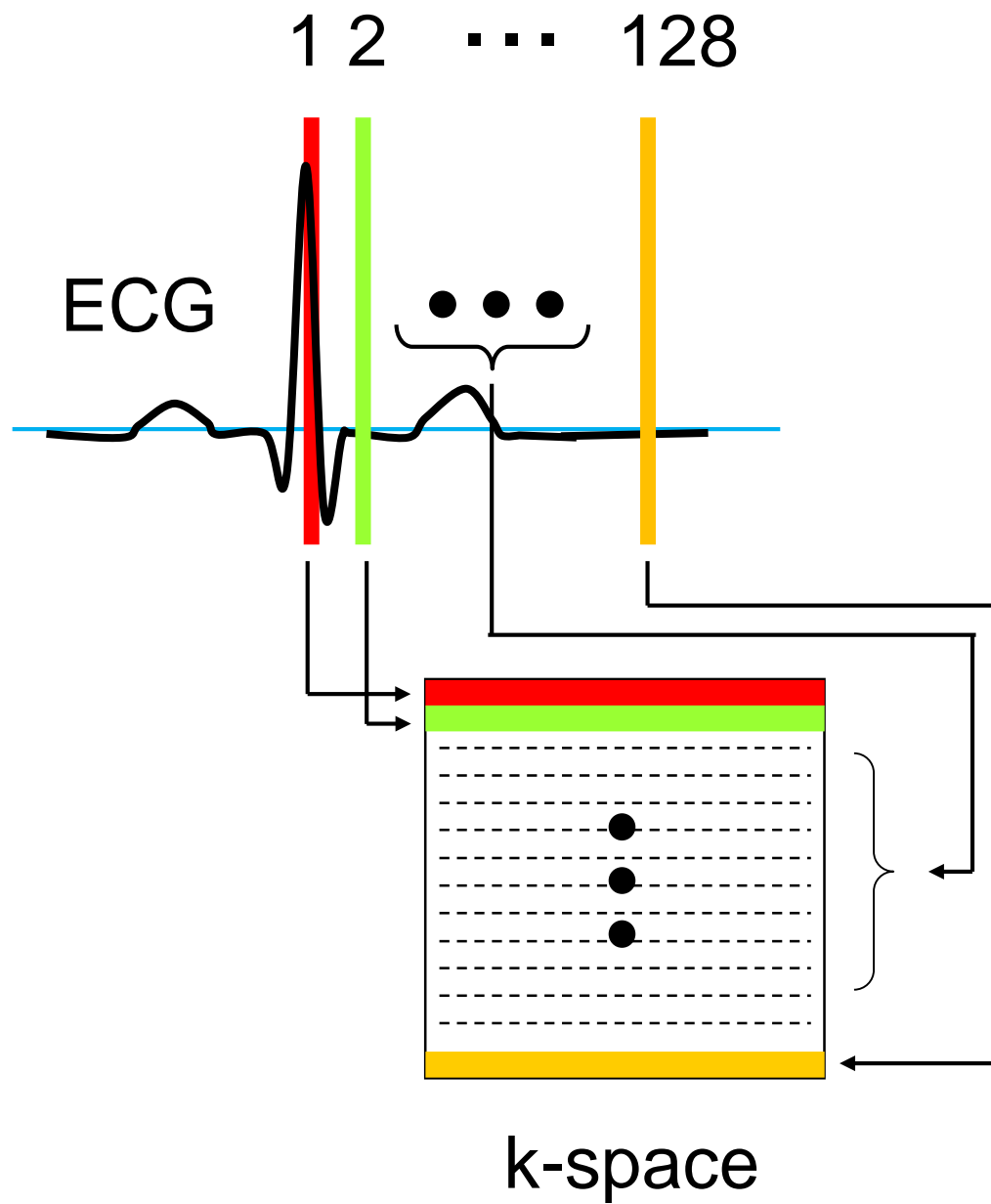


Figure 4

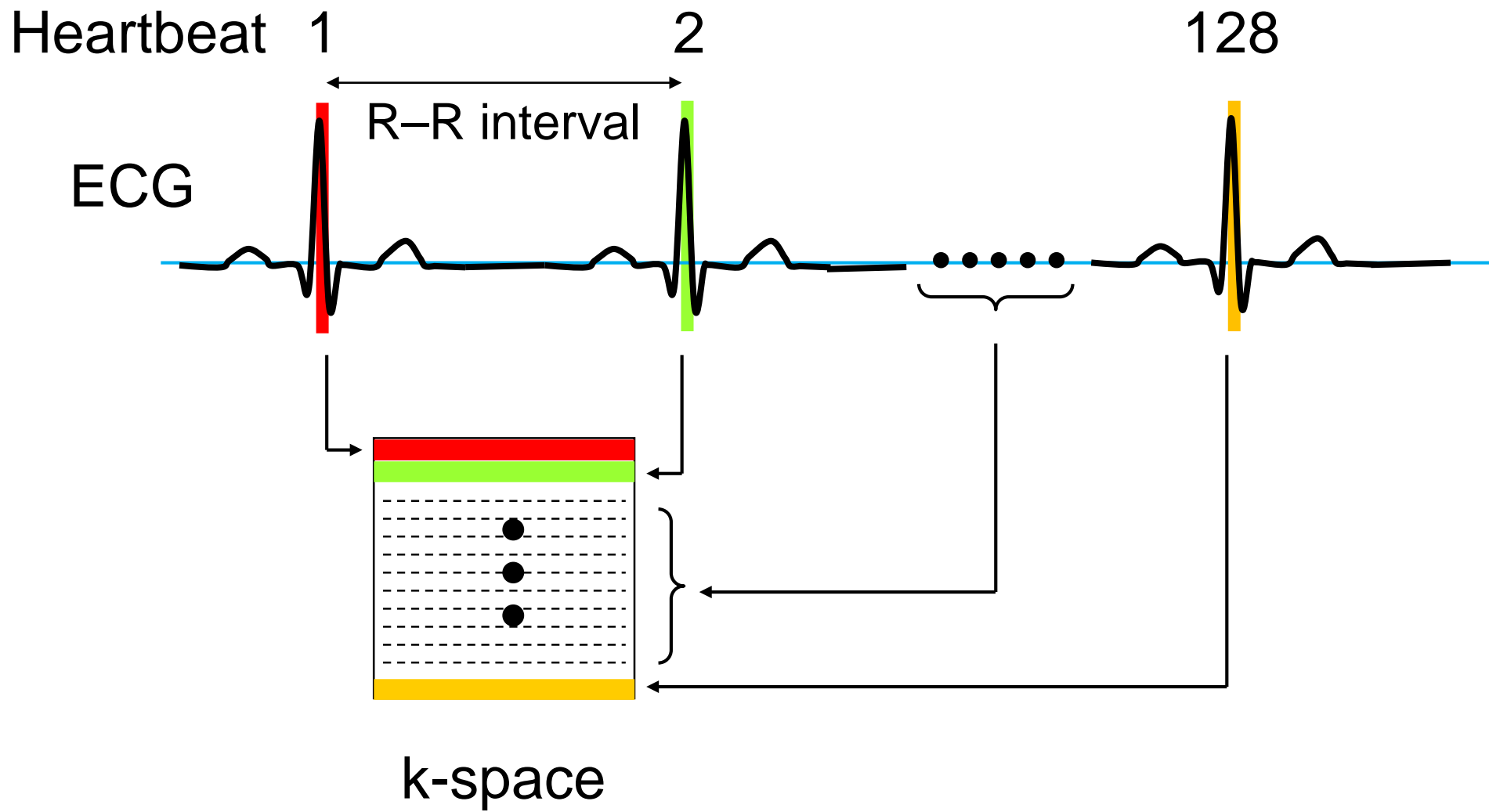


Figure 5

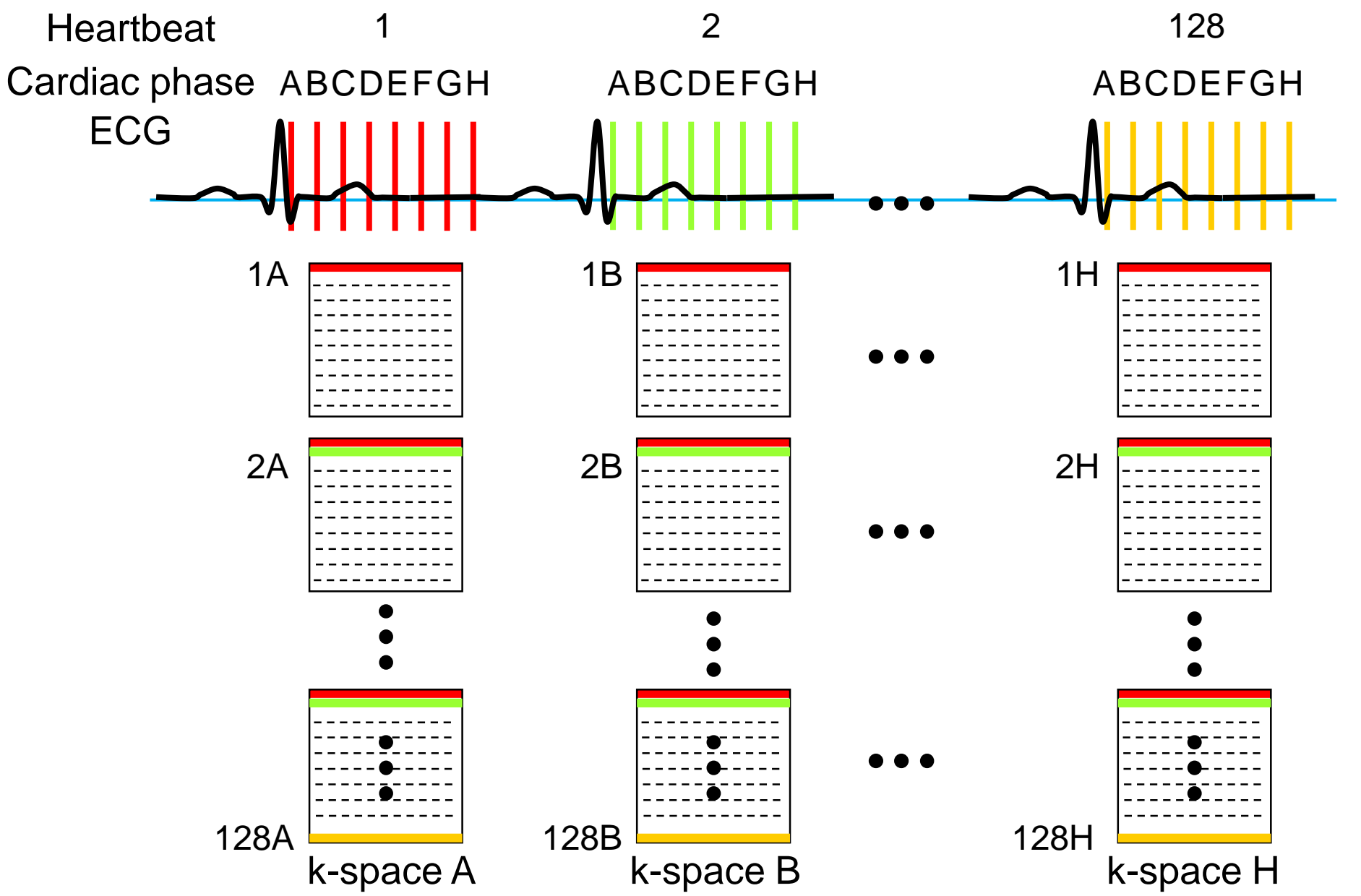


Figure 6

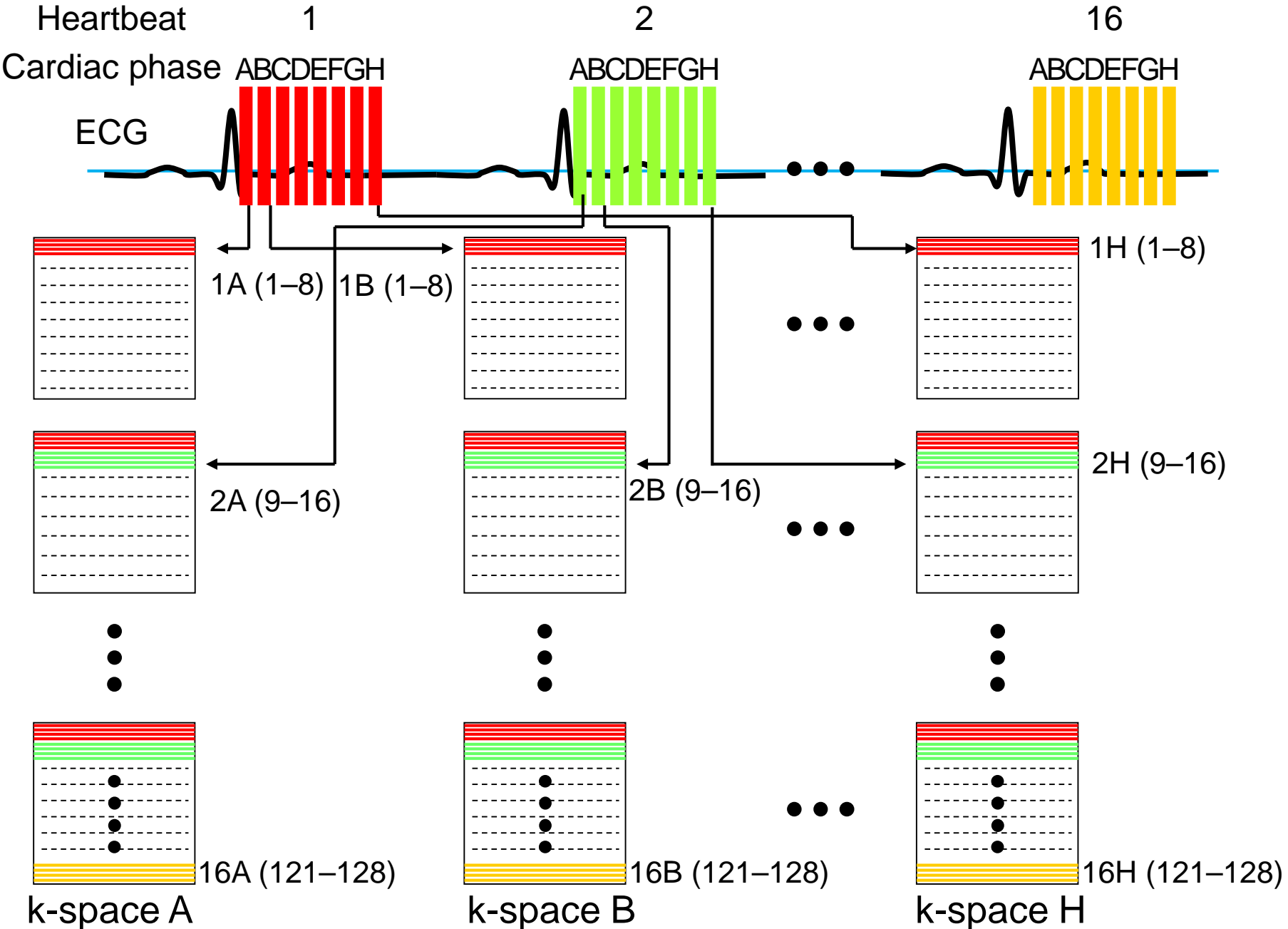


Figure 7

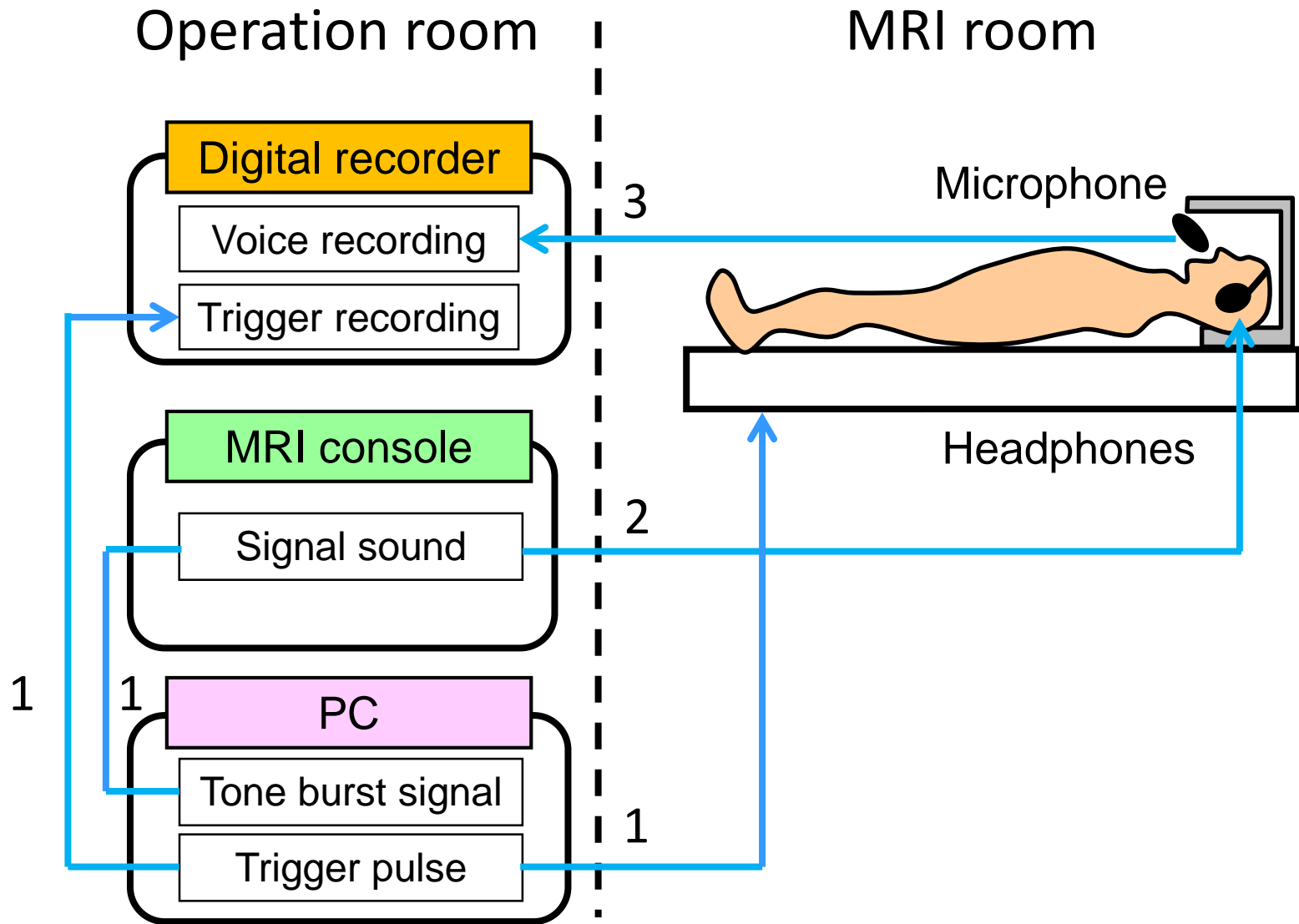


Figure 8

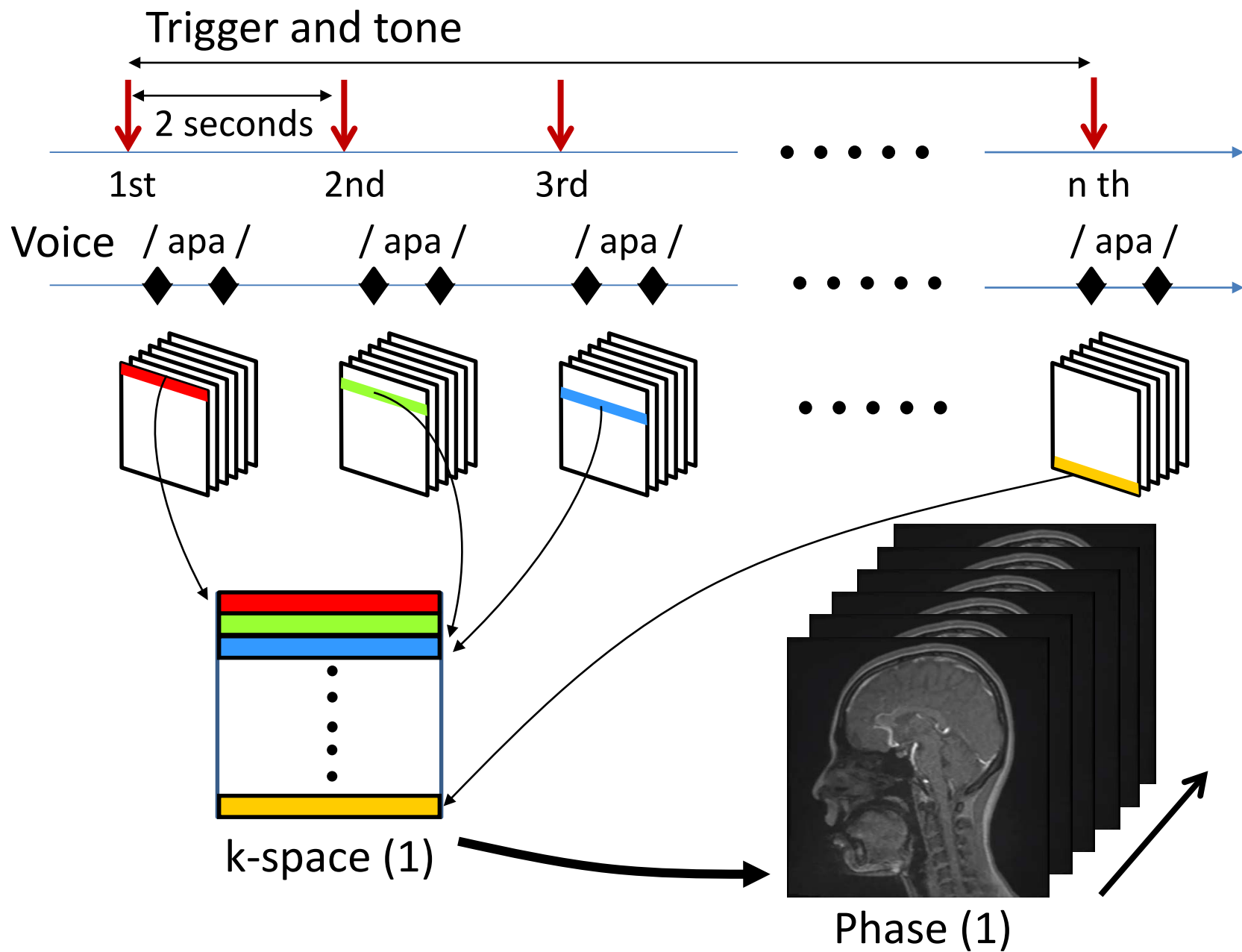


Figure 9

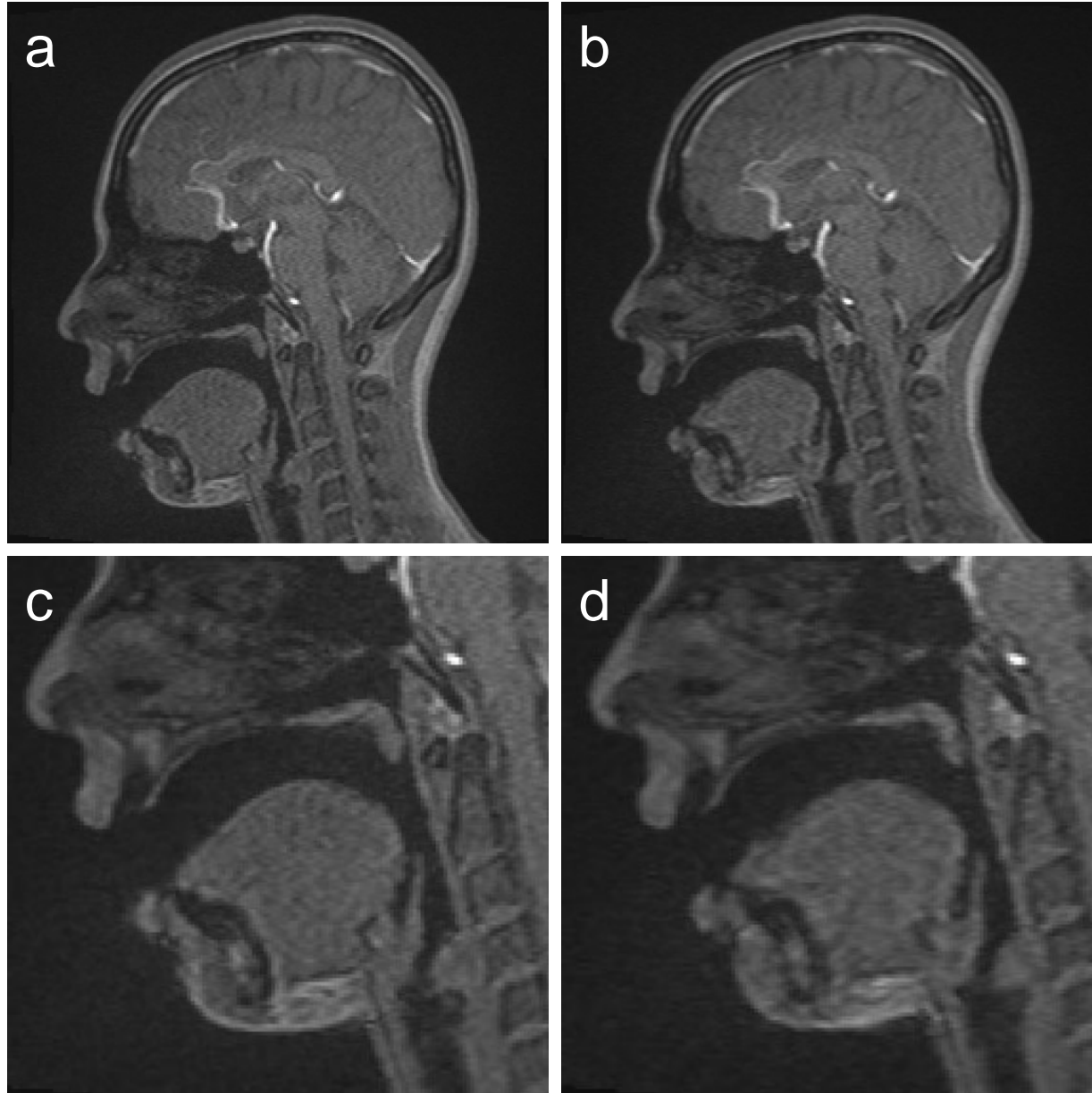


Figure 10

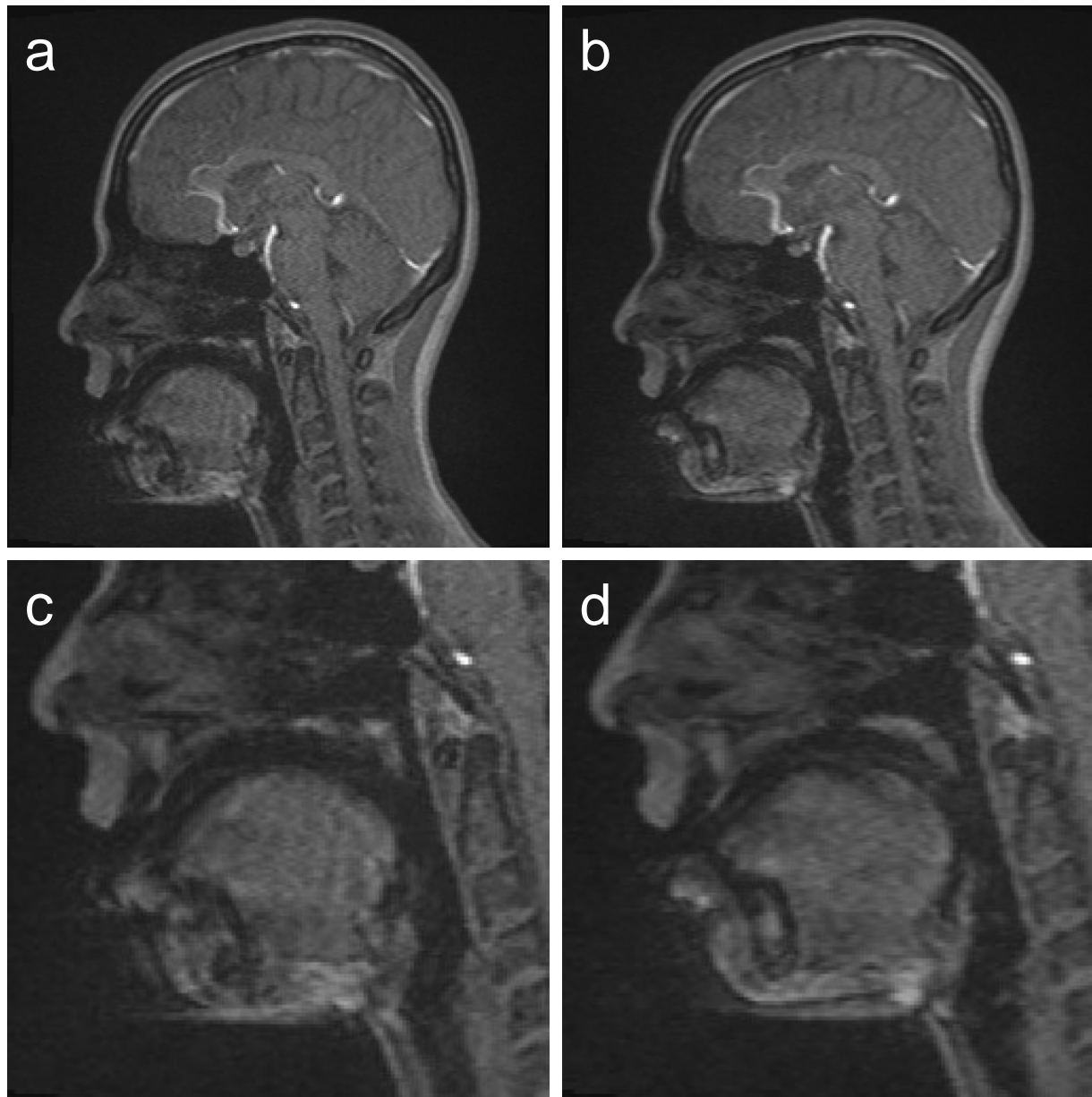


Figure 11

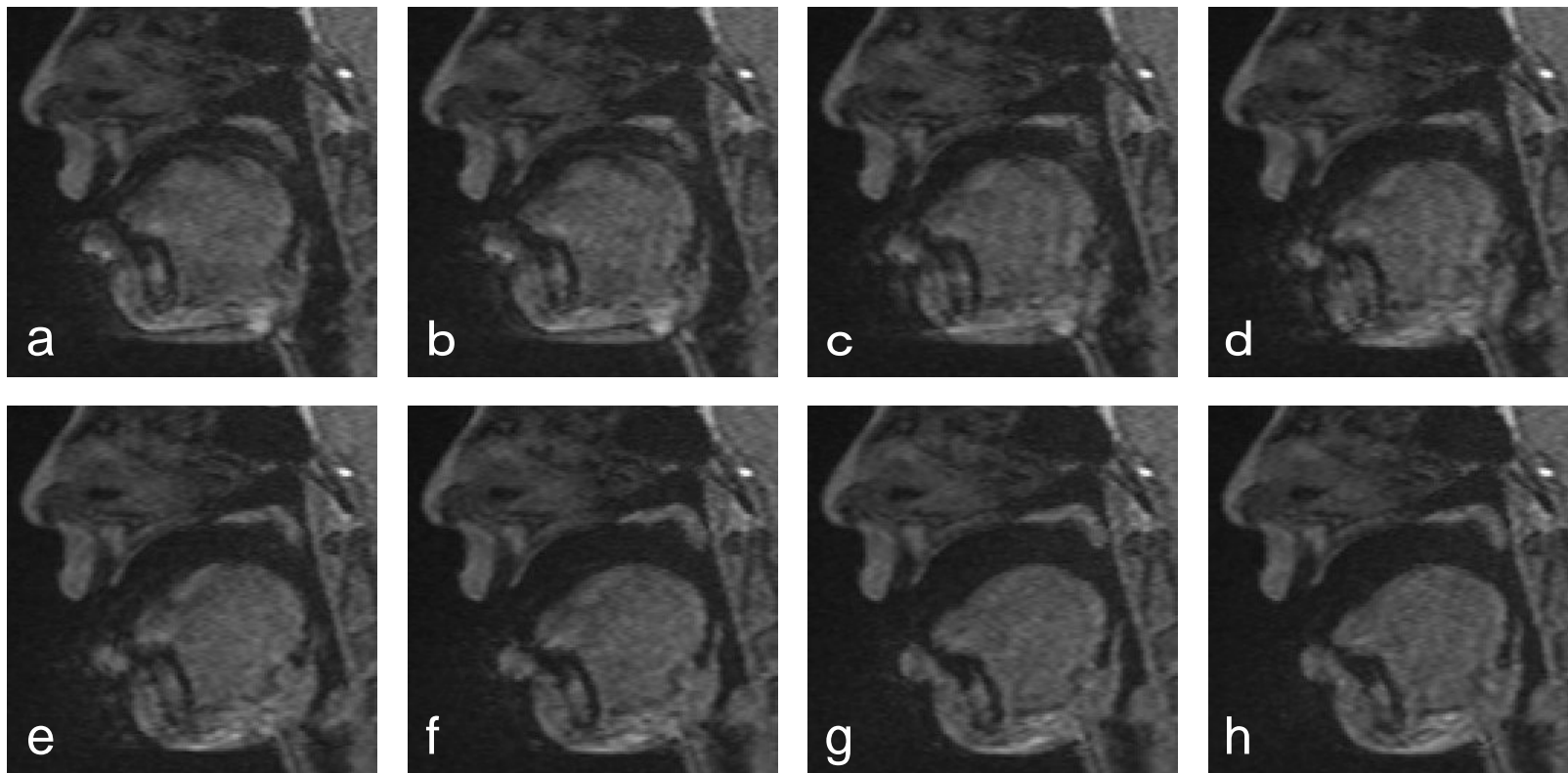


Figure 12

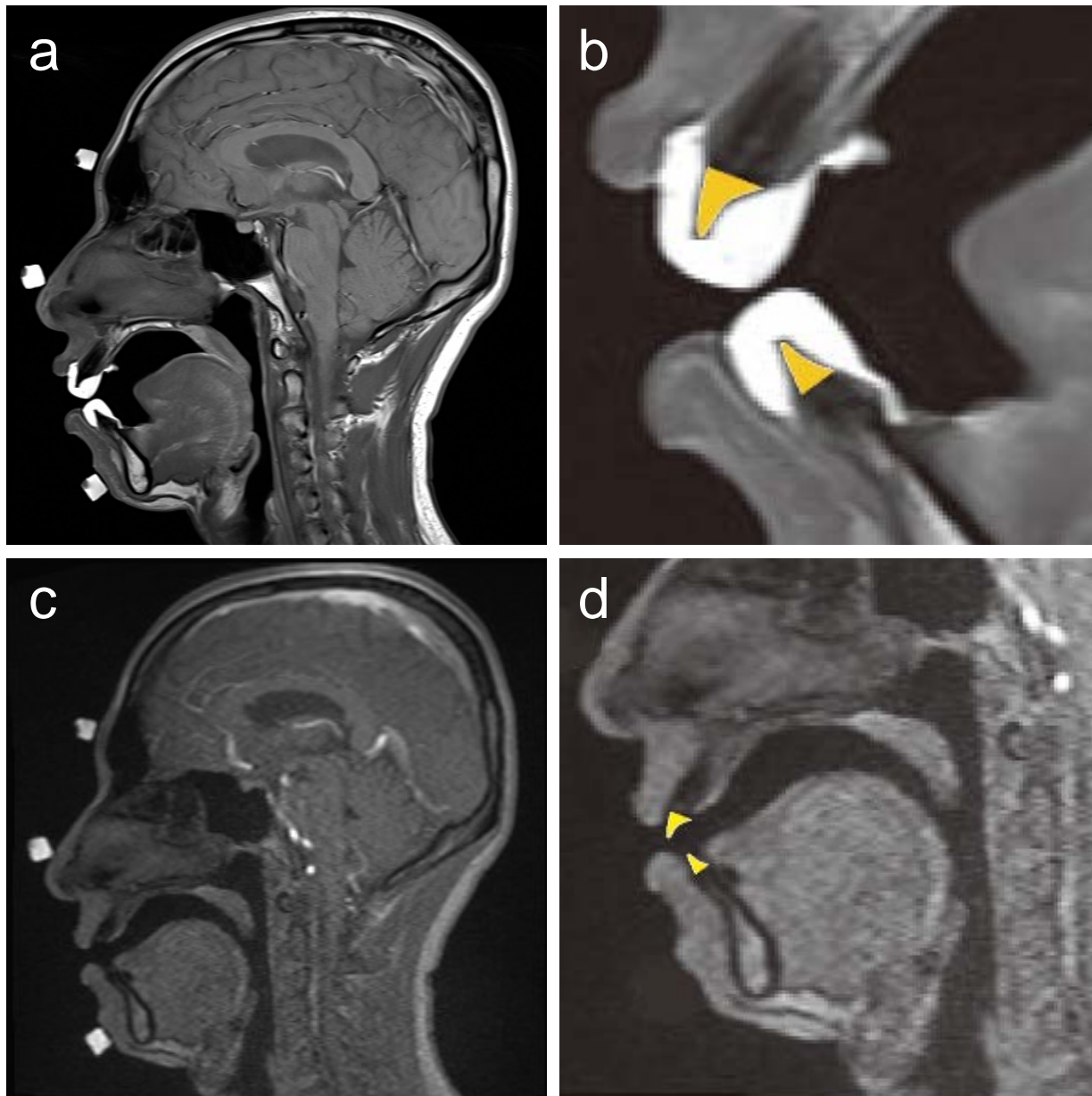


Figure 13

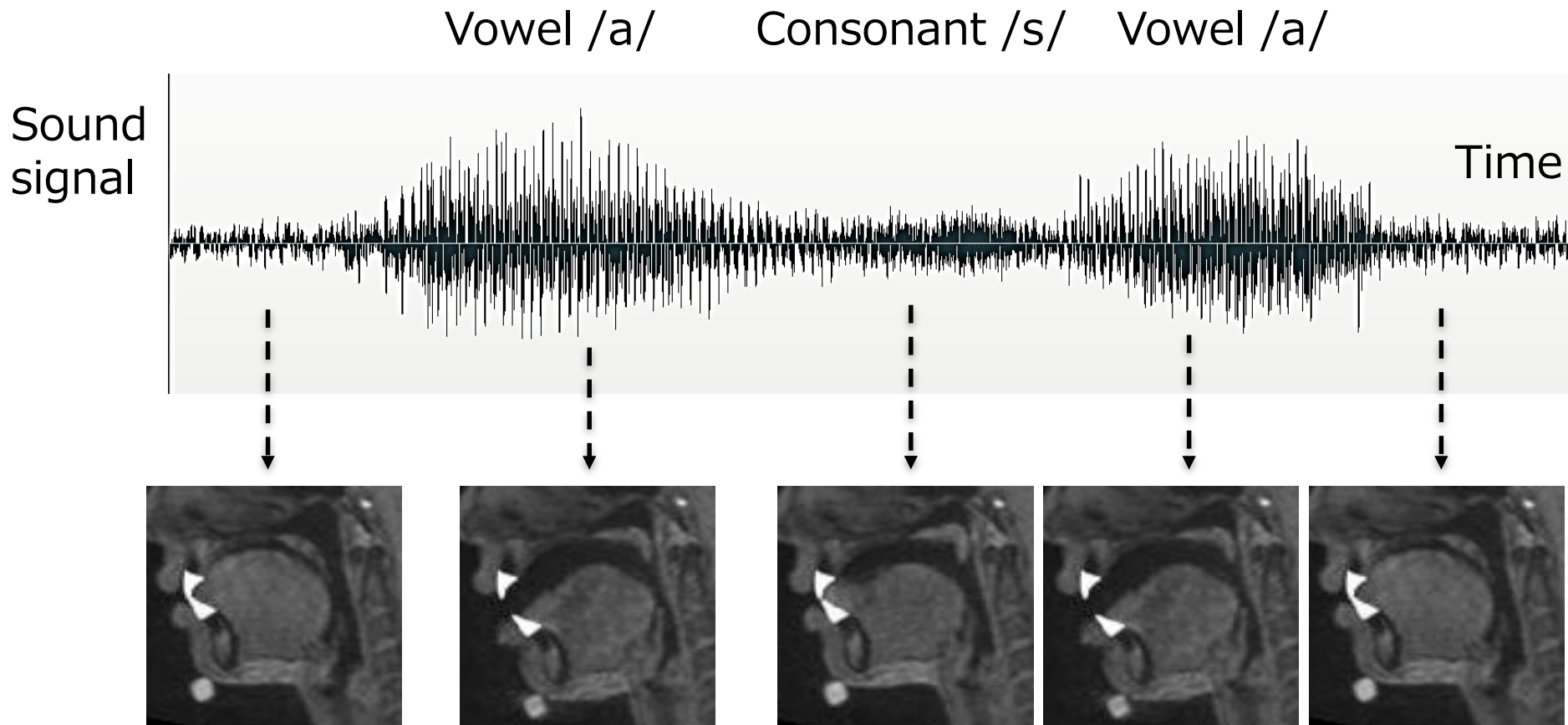


Figure 14

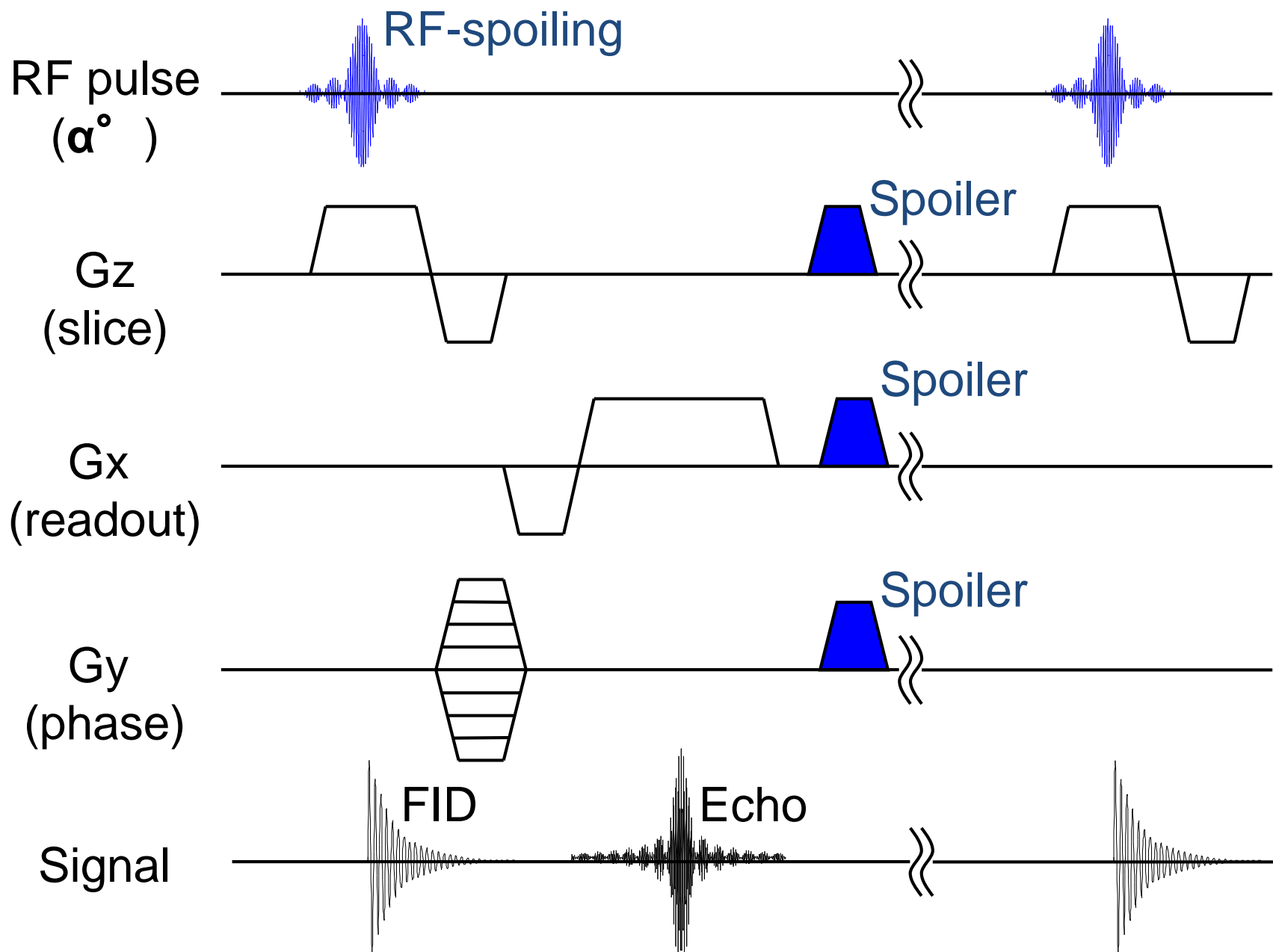


Figure 15

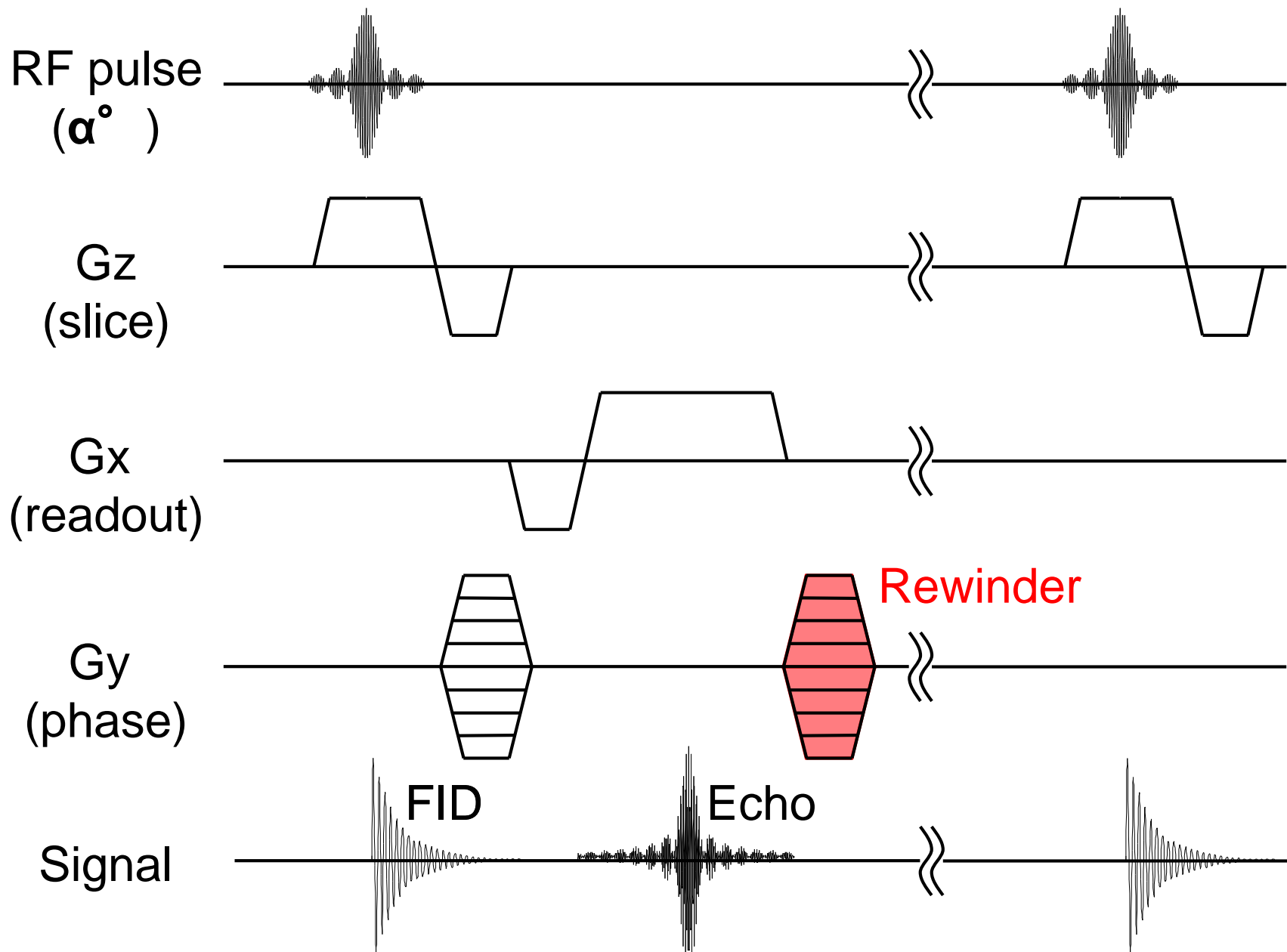


Figure 16

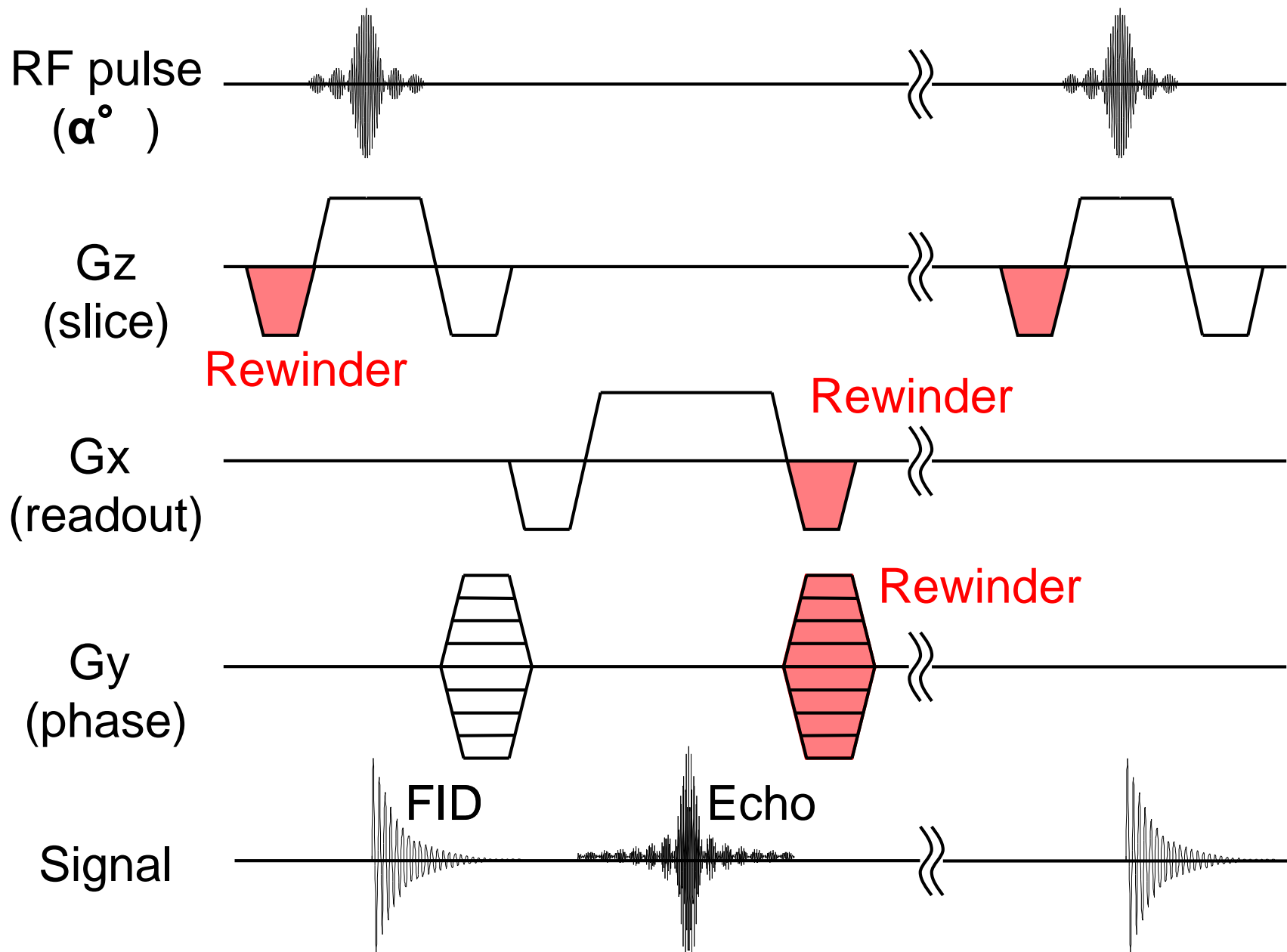


Figure 17

